Supporting Information

Synergistic engineering layer with versatile $H_2Ti_3O_7$ electrocatalyst for suppressed shuttle effect and enhanced catalytic conversion of lithium–sulfur batteries

Changhoon Choi[a], Jung Been Park[a], and Dong-Wan Kim*[a]

[a] *School of Civil, Environmental, and architectural Engineering, Korea University, Seoul 02841, South Korea*

Corresponding Author

*E-mail: dwkim1@korea.ac.kr (Prof. Dong-Wan Kim)

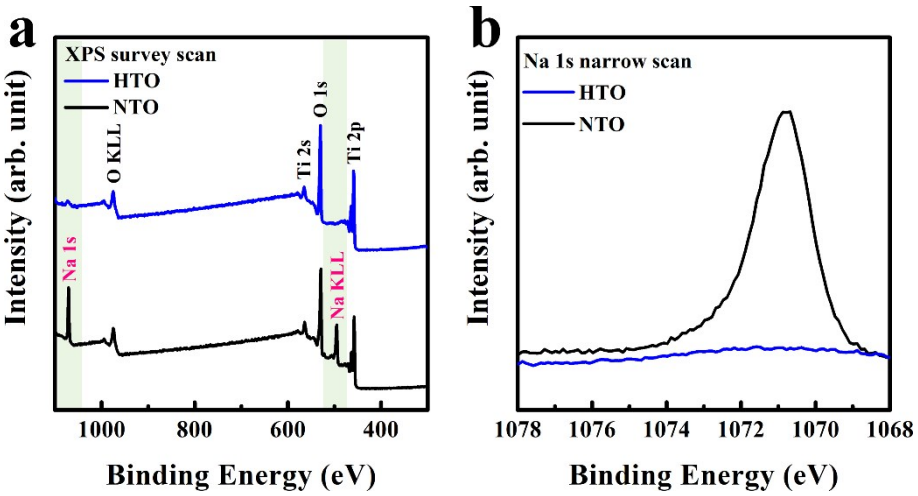

Figure S1. (a) XPS survey spectra and (b) Na 1s spectra of HTO and NTO.

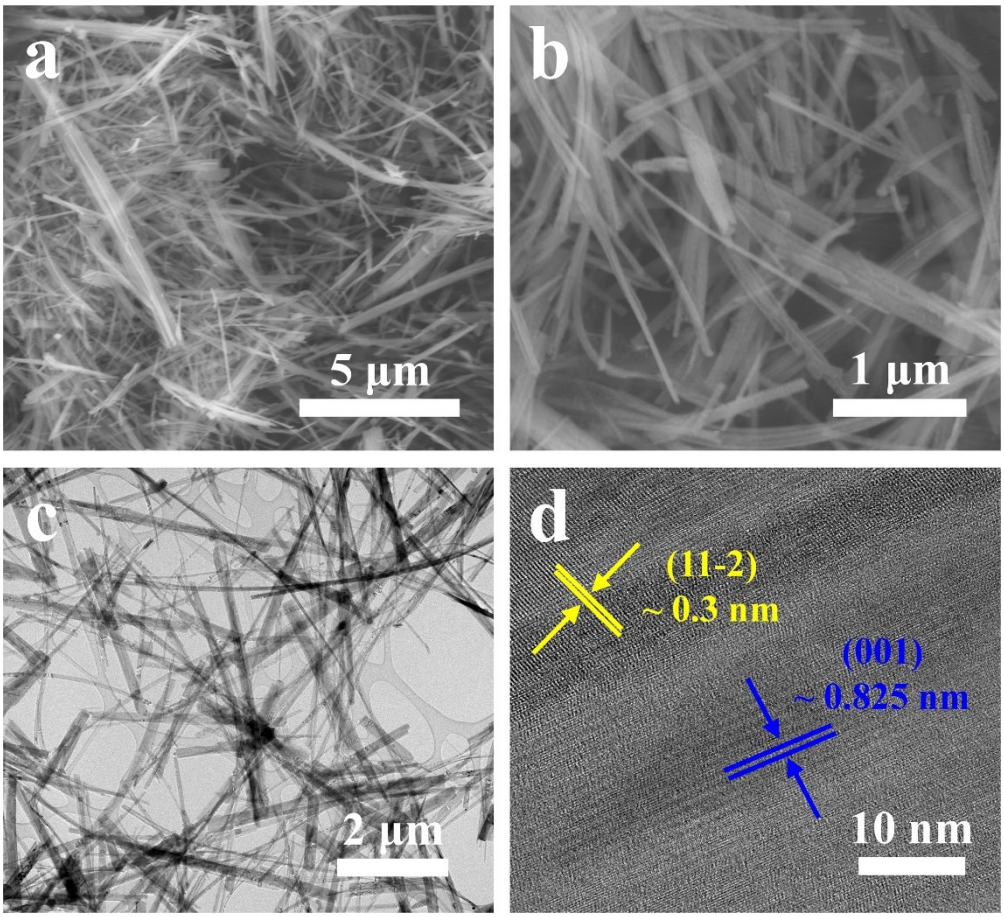

Figure S2. (a-b) SEM and (c) TEM images of NTO nanowires. (d) HR-TEM image of NTO nanowires.

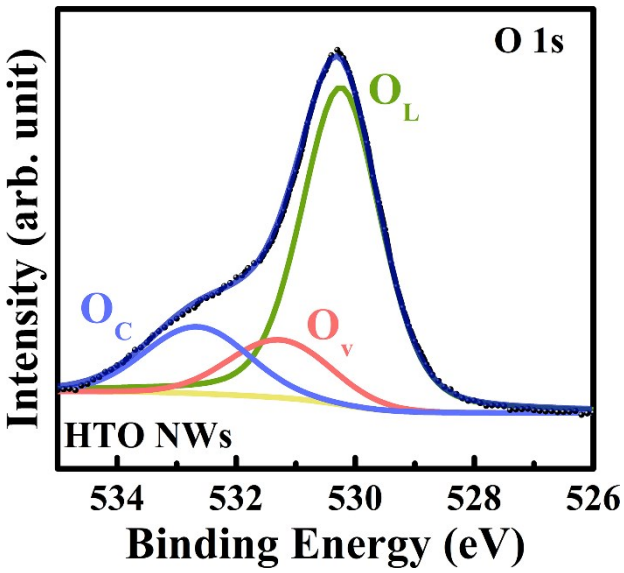

Figure S3. High-resolution XPS spectra of O 1s in HTO (O_L: lattice oxygen species, O_V: oxygen vacancies and defect, O_C: dissociated and chemisorbed oxygen in HTO).

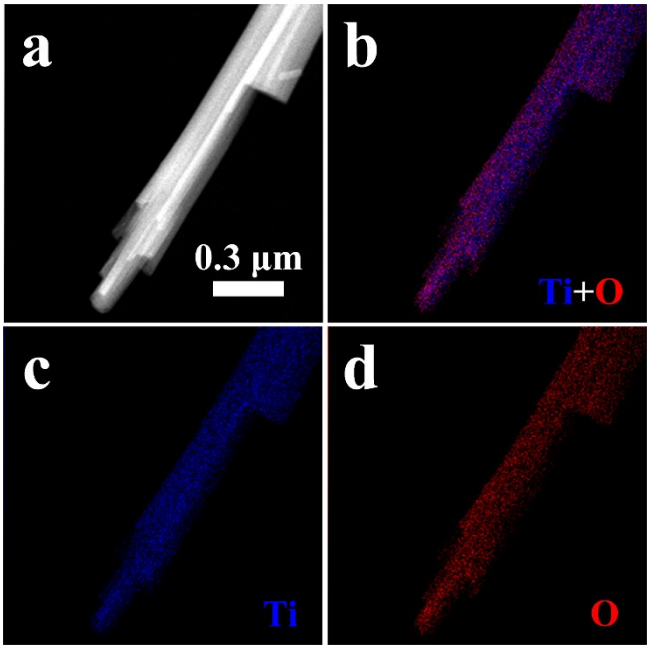

Figure S4. (a) EDX elemental mapping area and (b-d) corresponding elemental distributions of HTO nanowires.

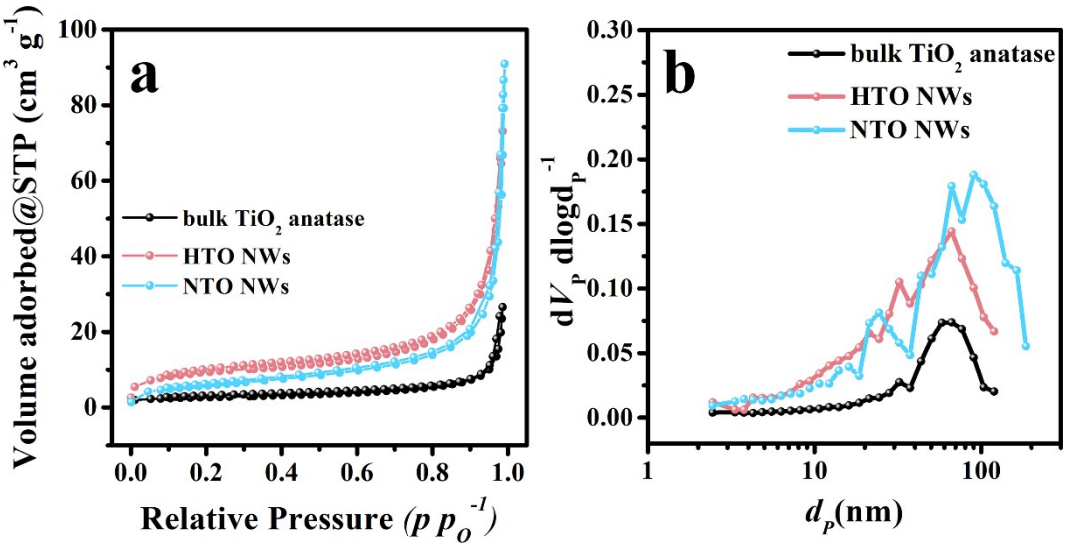

Figure S5. (a) N_2 adsorption-desorption isotherms and (b) Barrett-Joyner-Halenda (BJH) pore size distribution of bulk TiO_2 anatase, HTO, and NTO nanowires.

Table S1. The textural parameters of bulk TiO_2 anatase, HTO, and NTO nanowires.

Sample	Specific surface area (m^2 g^{-1})	Total pore volume (cm^3 g^{-1}, p/p_0=0.990)	Mean pore diameter (nm)
HTO NWs	34.11	0.1132	13.272
NTO NWs	20.90	0.1272	24.342
Bulk TiO_2 anatase	9.62	0.0411	17.084

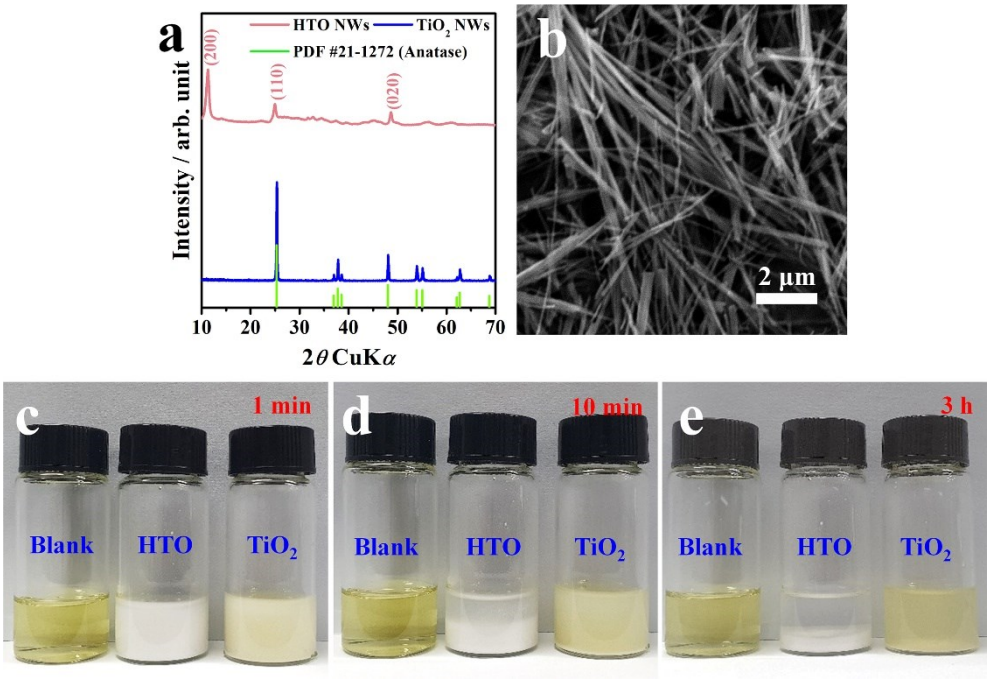

Figure S6. (a) XRD profiles of synthesized HTO and HTO-derived TiO_2. (b) SEM image of HTO-derived TiO_2 nanowires. Optical photographs of Li_2S_6 solution after the addition of HTO and HTO-derived TiO_2 nanowires for (c) 1 min, (d) 10 min, and (e) 3 h.

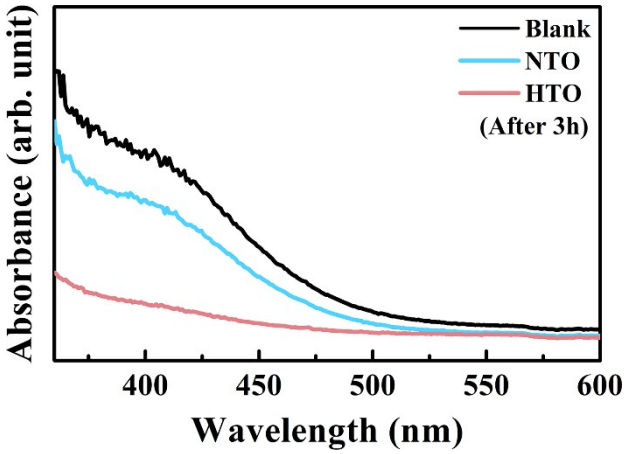

Figure S7. UV-vis absorbance spectra of blank Li_2S_6 solution and the supernatant of Li_2S_6 solutions after the addition of NTO and HTO for 3 h as shown in Figure 2c.

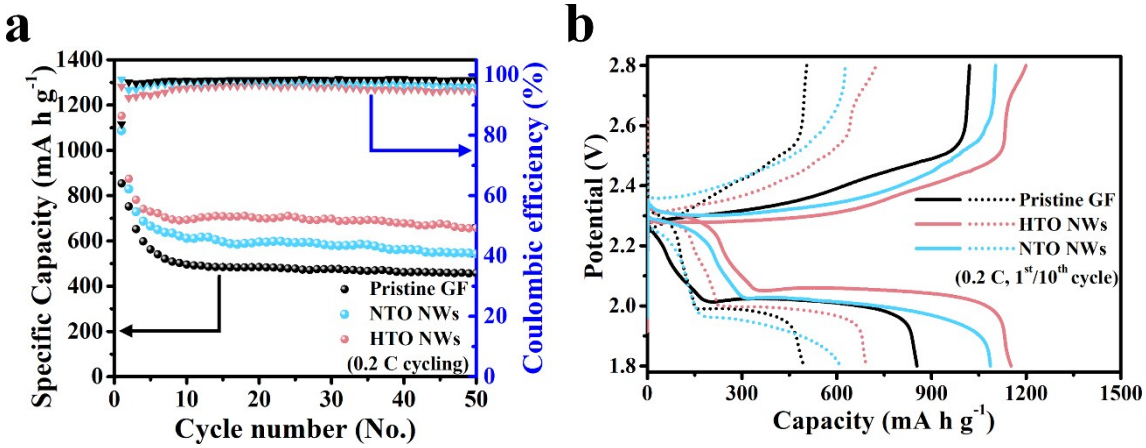

Figure S8. (a) Cycling performance and (b) galvanostatic profiles of Li-S batteries with pristine GF, NTO-coated separator, and HTO-coated separator at 0.2 C.

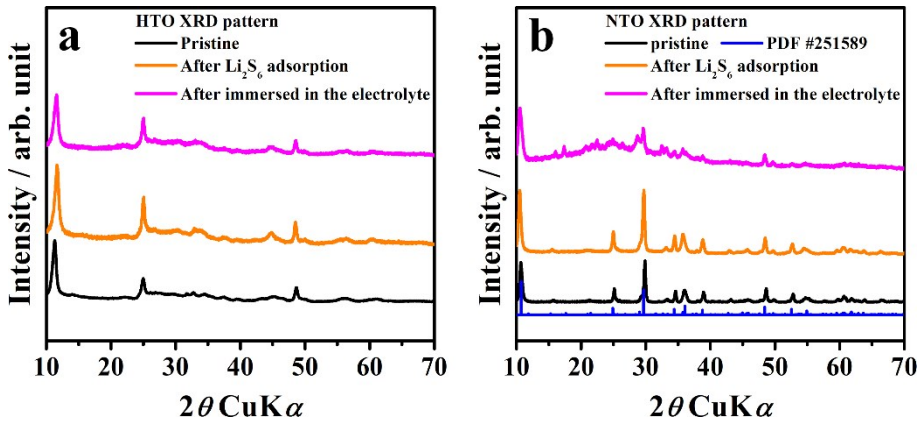

Figure S9. Chemical integrity test of (a) HTO and (b) NTO with XRD patterns of the dried powders after Li_2S_6 adsorption test and after immersed in electrolyte (1 M LiTFSI in DOL/DME with 0.2 M $LiNO_3$) for 24 h.

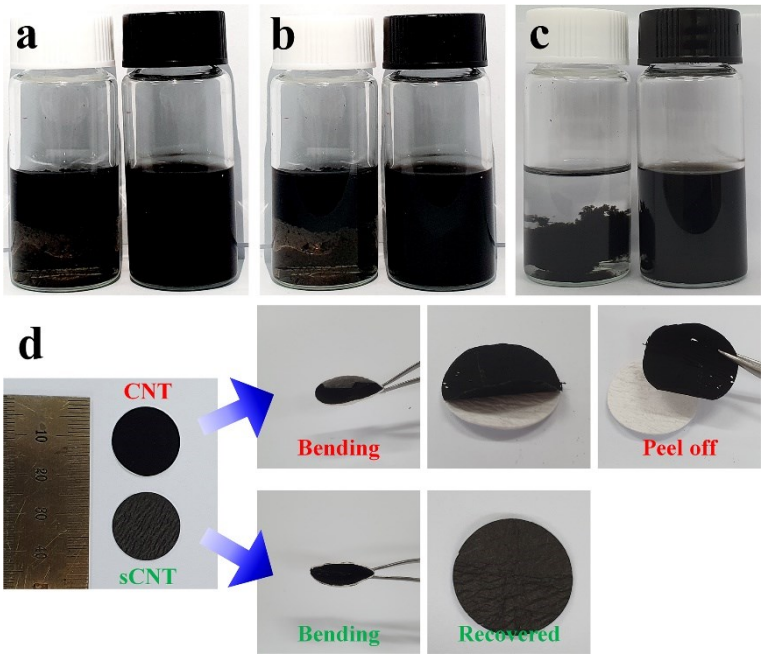

Figure S10. Digital images of ultrasonicated coating ink of CNT (left) and sCNT(right) (a) after 0 min, (b) 30 min and (C) 24 h. (d) Bending test of modified separators with CNT and sCNT.

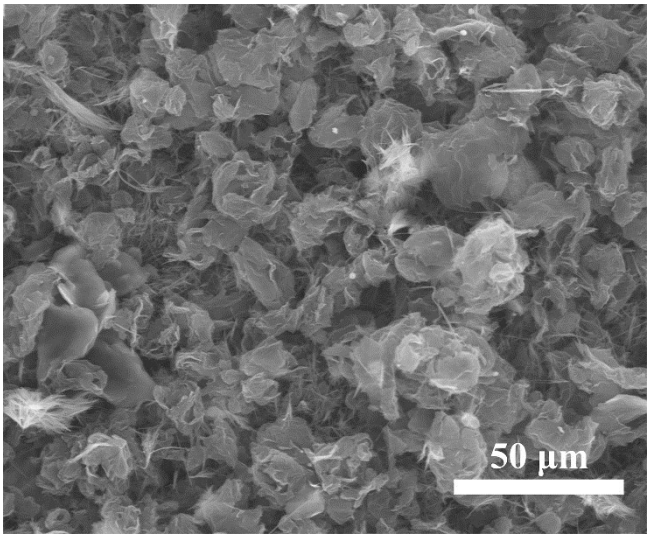

Figure S11. Low-magnification top-view SEM image of HTO-sCNT-G engineering layer.

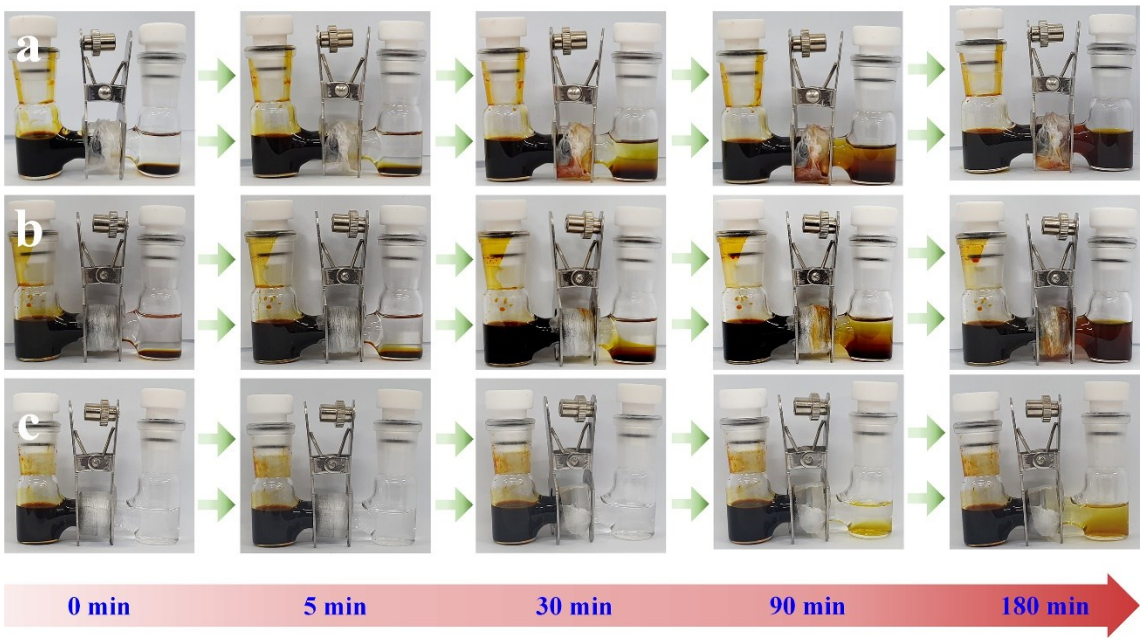

Figure S12. H-cell type PS permeation test of (a) pristine GF, (b) sCNT-coated GF, and HTO-sCNT-coated GF for 3 h.

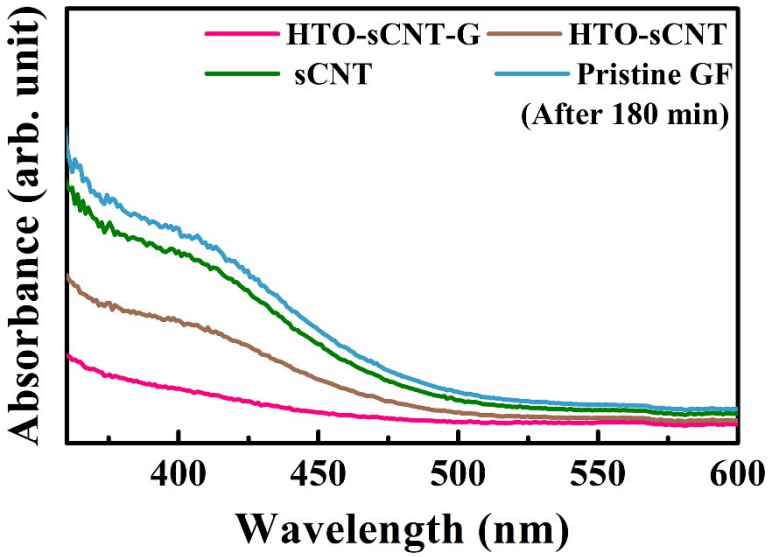

Figure S13. UV-vis spectra of the solvent on the right compartment of H-cell after H-cell type PS permeation test for 180 min.

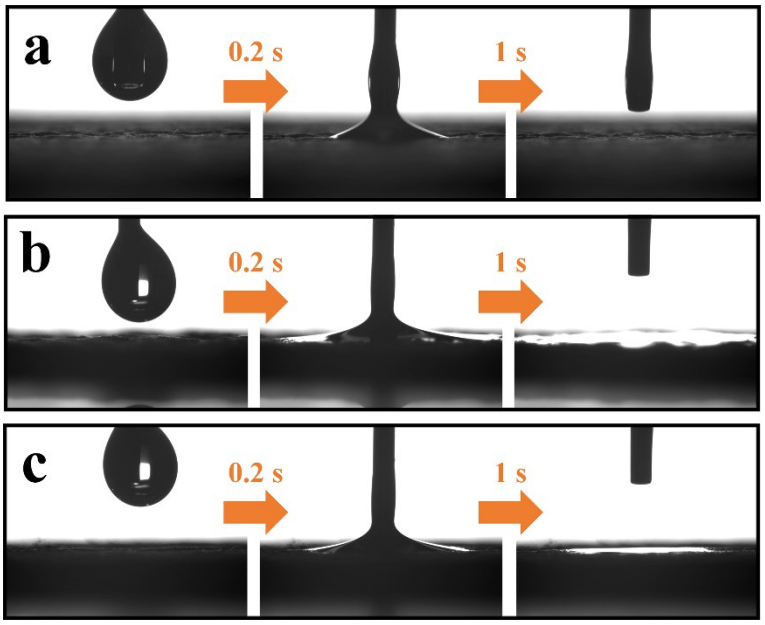

Figure S14. Contact angle photographs of (a) pristine GF, and modified separators with (b) HTO-sCNT and (c) HTO-sCNT-G using liquid electrolyte.

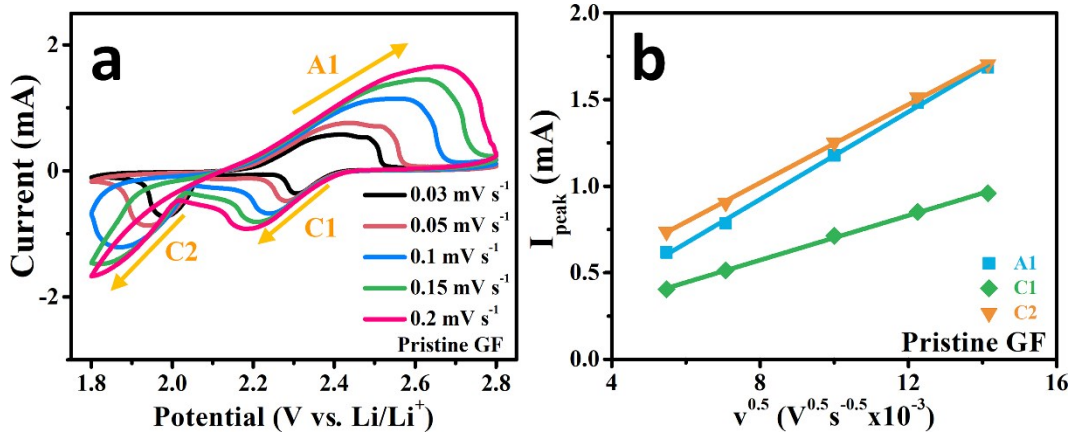

Figure S15. Cyclic voltammograms of Li-S batteries with (a) pristine GF at different voltage scan rates (0.03-0.2 mV s^{-1}) and (b) the corresponding linear fits.

Table S2. A summary of Li^+ diffusion coefficients of pristine GF, GF modified with HTO-sCNT and HTO-sCNT-G within Li-S batteries.

Calculated parameters	**Pristine GF**	**HTO-sCNT**	**HTO-sCNT-G**
D_{Li+} at Al (cm^2 s^{-1})	4.472×10^{-8}	1.790×10^{-7}	3.188×10^{-7}
D_{Li+} at Cl (cm^2 s^{-1})	1.163×10^{-8}	1.317×10^{-7}	1.376×10^{-7}
D_{Li+} at C2 (cm^2 s^{-1})	3.589×10^{-8}	1.599×10^{-7}	2.215×10^{-7}

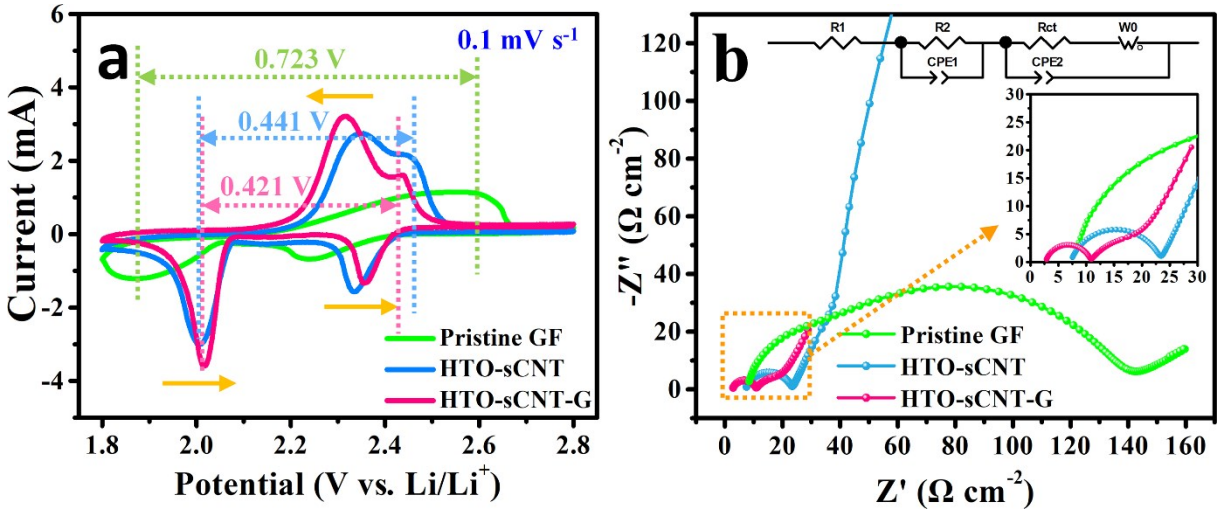

Figure S16. (a) Typical Cyclic voltammograms of Li-S batteries with different separators at a scan rate of 0.1 mV s^{-1}. (b) electrochemical impedance spectroscopy (EIS) of Li-S batteries with different separators at open-circuit voltage. (R_1 - intercept at a higher frequency on the real $\dot{Z}$ axis, R_2 - semicircle at high frequency, R_{ct} - semicircle in middle frequency, and W_o – sloping line in the low frequency)

Table S3. A summary of the fitted parameters of EIS plots in Figure S11b.

	R_1 (Ω)	R_2 (Ω)	R_{ct} (Ω)
Pristine GF	7	17	113.5
HTO-sCNT	7.1	16.2	18.0
HTO-sCNT-G	2.7	8.1	13.0

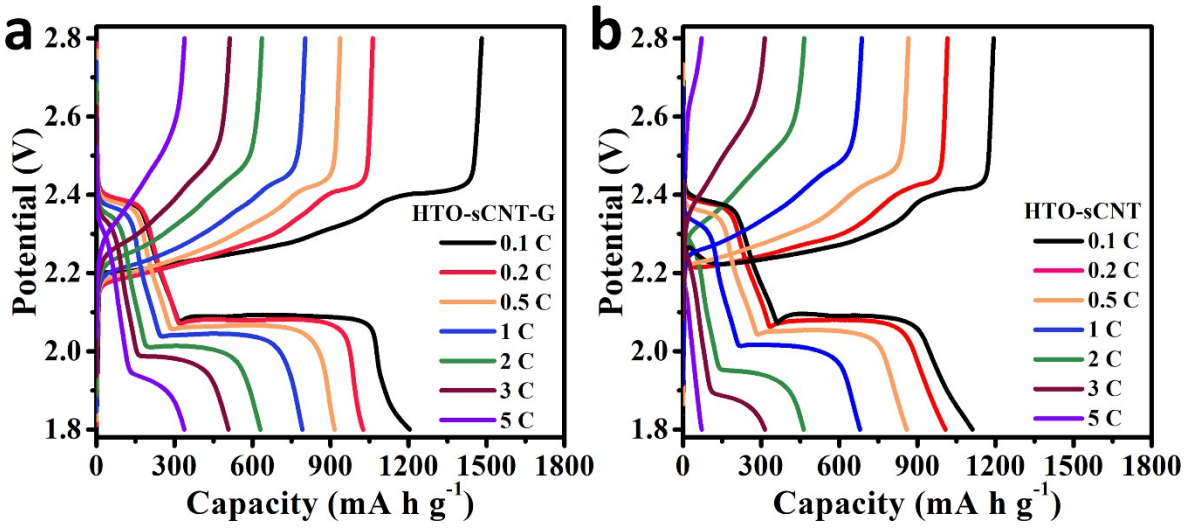

Figure S17. Galvanostatic charge/discharge profiles of Li-S batteries with (a) HTO-sCNT-G and (b) HTO-sCNT at stepwise current rates from 0.1 to 5 C.

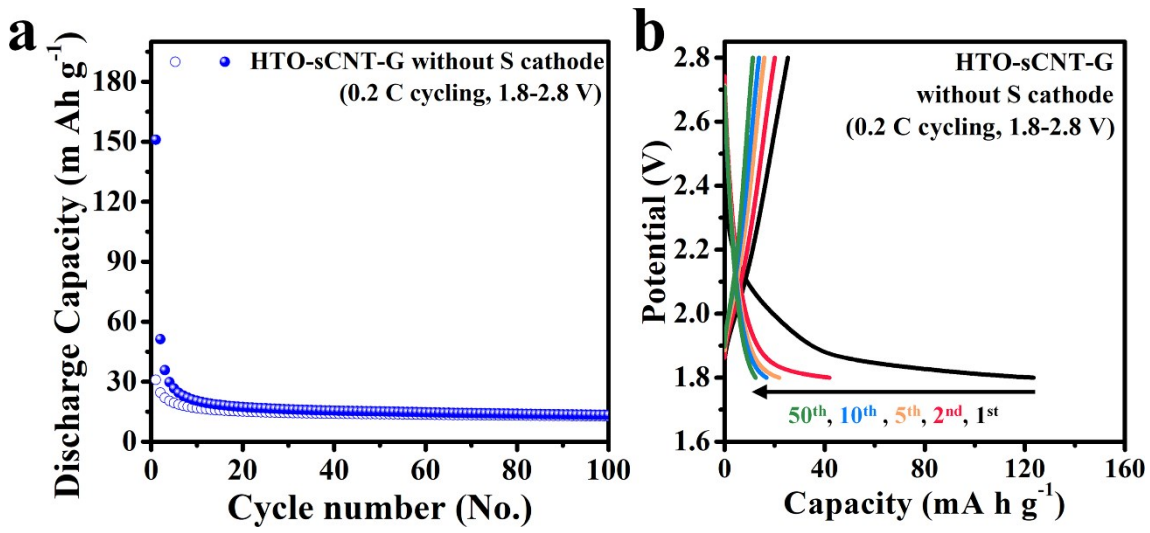

Figure S18. (a) Cycling performance and (b) galvanostatic charge/discharge profiles of HTO-sCNT-G without S cathode under the same 0.2 C cycling test condition as figure 5d.

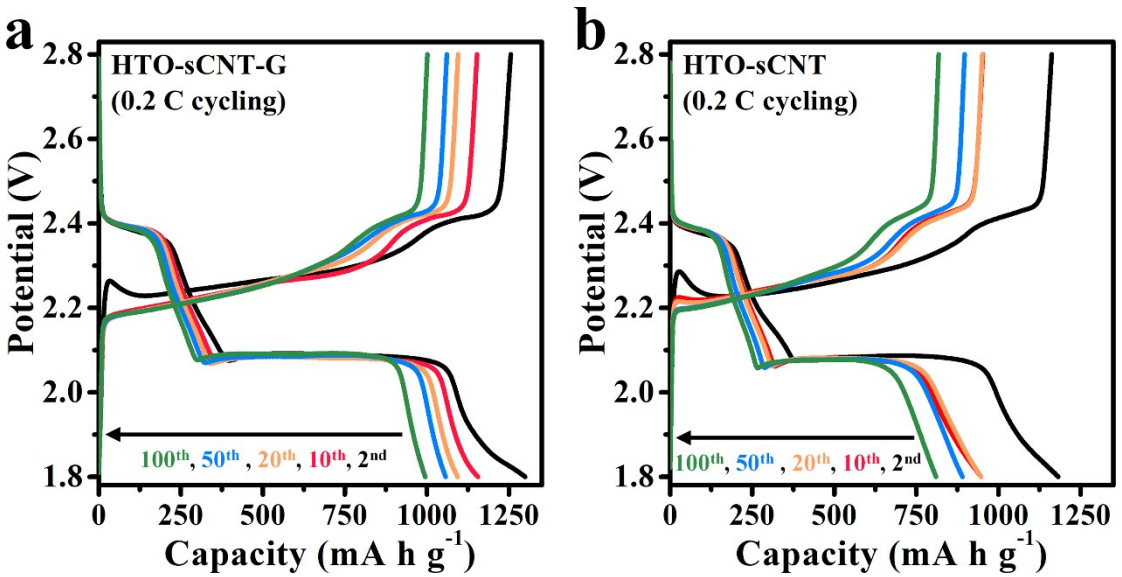

Figure S19. Galvanostatic profiles of Li-S batteries with (a) HTO-sCNT-G and (b) HTO-sCNT for different cycles at 0.2 C.

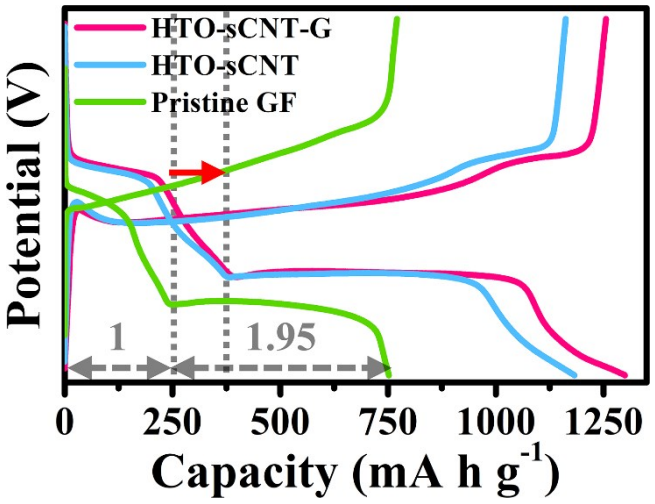

Figure S20. Typical galvanostatic profiles of Li-S batteries with pristine GF, HTO-sCNT, and HTO-sCNT-G for the 2nd cycle at 0.2 C.

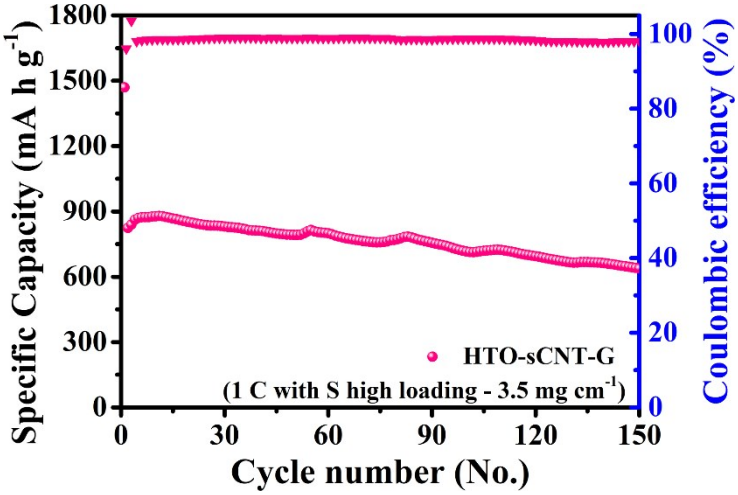

Figure S21. Cycling performance of the cell with HTO-sCNT-G using high loading sulfur cathode (~3.5 mg cm^{-1}) at 1 C for 150 cycles.

Table S4. An electrochemical performance comparison of Li-S batteries with representative interlayers and modified separators, with result from this work (HTO-sCNT-G) and from previously related papers.

Materials	Cathode (S loading wt%)	C-rate	Cycle numbers	Specific capacity (mA h g^{-1})	Long-term cycle stability	Ref
HTO-sCNT-G	Pure sulfur/Ketjen black (75 wt%)	0.2C	100	1001	1C, 500 cycles, 794 mA h g^{-1} (0.057% decay per cycle)	(This work)
Nano TiO_2-Carbon	Pure sulfur/Acetyclene black (63 wt%)	0.1C	180	883	0.5C, 200 cycles, 762 mA h g^{-1}	31
Electrospun Ti_4O_7-Carbon	[M] CMK3/S-Acetyclene black (60 wt%)	0.2C	100	945	1C, 1000 cycles, 560 mA h g^{-1}	33
TiO_2-C-MoS_2	Pure sulfur/Super P (60 wt%)	0.2C	100	634	1C, 1500 cycles, 501 mA h g^{-1} (0.039% decay per cycle)	40
Prussian Blue	[M] Pure sulfur/Ketjen black (75 wt%)	0.2C	100	820.7	1C, 1000 cycles, 537 mA h g^{-1} (0.03% decay per cycle)	67
Ni@NG-CNTs	Pure sulfur/Super P (70 wt%)	0.2C	200	783	1C, 800 cycles, 655.5 mA h g^{-1} (0.054% decay per cycle)	S1
CoS-Co_9S_8-CCNSs	Pure sulfur/Ketjen black (70 wt%)	0.2C	100	911.3	1C, 500 cycles, 600 mA h g^{-1} (0.018% decay per cycle)	S2
VO_x-Graphene	Pure sulfur/Carbon black (80 wt%)	0.2C	200	738	1C, 600 cycles, 441 mA h g^{-1} (0.069% decay per cycle)	S3
$MnFe_2O_4$-Acetyclene black	[M] Pure sulfur/Ketjen black (76.9 wt%)	0.5C	200	743	1C, 500 cycles, 625 mA h g^{-1} (0.074% decay per cycle)	S4
WS_2-Carbon	Pure sulfur/Super P (70 wt%)	0.5C	300	816	1C, 1000 cycles, 416 mA h g^{-1} (0.045% decay per cycle)	S5
Ni_3Fe-N doped carbon	Pure sulfur/Super P (70 wt%)	0.2C	200	821	1C, 1000 cycles, 591 mA h g^{-1} (0.034% decay per cycle)	S6
Ketjen black – mesoporous TiO_2	[M] Pure sulfur/Ketjen black (unkown, 0.7 mg cm^{-2})	0.2C	60	991.8	0.5C, 100 cycles, 804.3 mA h g^{-1}	S7
MWCNTs - TiO_2 quantum dots	Pure sulfur/Carbon black (60 wt%)	-	-	-	0.5C, 600 cycles, 610 mA h g^{-1} (0.072% decay per cycle)	S8
Carbon@Ti_4O_7 non-woven fabric	Pure Sulfur/Black pearls (70 wt%)	1C	200	721	2C, 500 cycles, 562 mA h g^{-1} (0.09% decay per cycle)	S9
TiO_2 – Carbon (praline-like)	[M] Pure sulfur/MWCT (70 wt%)	-	-	-	0.2C, 300 cycles, 770.8 mA h g^{-1} (0.2% decay per cycle)	S10

[M]: Use typical melt-deffusion method to prepare sulfur cathode.

Reference for Supporting Information

S1. X. T. Zuo, M. M. Zhen and C. Wang, *Nano Res*, 2019, **12**, 829-836.

S2. S.-D. Seo, C. Choi, D. Park, D.-Y. Lee, S. Park and D.-W. Kim, *Chem Eng J*, 2020, **400**, 125959.

S3. Y. Z. Zhang, X. Ge, Q. Kang, Z. K. Kong, Y. L. Wang and L. Zhan, *Chem Eng J*, 2020, **393**, 124570.

S4. Y. Wang, X. Guo, C. Chen, Y. Wang, Q. Li, Z. Wu, B. Zhong and Y. Chen, *Electrochim Acta*, 2020, **354**, 136704.

S5. S. Ali, M. Waqas, X. P. Jing, N. Chen, D. J. Chen, J. Xiong and W. D. He, *Acs Appl Mater Inter*, 2018, **10**, 39417-39421.

S6. Z. Zhang, A. H. Shao, D. G. Xiong, J. Yu, N. Koratkar and Z. Y. Yang, *Acs Appl Mater Inter*, 2020, **12**, 19572-19580.

S7. S. Lin, Y. R. Cai, J. Yang, F. X. Ruan, J. Wu, S. Babu, X. Yao, J. K. Gao and J. M. Yao, *J Alloy Compd*, 2019, **779**, 412-419.

S8. H. B. Ding, Q. F. Zhang, Z. M. Liu, J. Wang, R. F. Ma, L. Fan, T. Wang, J. G. Zhao, J. M. Ge, X. L. Lu, X. Z. Yu and B. G. Lu, *Electrochim Acta*, 2018, **284**, 314-320.

S9. H. Tang, S. S. Yao, S. K. Xue, M. Q. Liu, L. L. Chen, M. X. Jing, X. Q. Shen, T. B. Li, K. S. Xiao and S. B. Qin, *Electrochim Acta*, 2018, **263**, 158-167.

S10. T. Zhao, Y. S. Ye, C. Y. Lao, G. Divitini, P. R. Coxon, X. Y. Peng, X. He, H. K. Kim, K. Xi, C. Ducati, R. J. Chen, Y. J. Liu, S. Ramakrishna and R. V. Kumar, *Small*, 2017, **13**, 1700357.